49th AIAA/ASME/ASCE/AHS/ASC Structures, Structural Dynamics, and Materials Conference
 16t
7 - 10 April 2008, Schaumburg, IL

AIAA 2008-2014

Influence of Cross-Sectional Geometry on Crush Characteristics of Multi-cell Prismatic Columns

Ali Najafi[1] and Masoud Rais-Rohani[2]
Department of Aerospace Engineering, Mississippi State University, Mississippi State, MS 39762

Analytical techniques founded on mechanics of progressive collapse of thin-walled structures and nonlinear transient dynamic finite element (FE) simulations are used to study the influence of cross-sectional geometry on the crush characteristics of multi-cell prismatic columns made of ductile materials. An analytical formula for the prediction of mean crush force is derived based on the super folding element model and the associated kinematically consistent representation of plastic collapse in the corner regions. In this model, the isotropic material is treated as rigid-perfectly plastic and the total internal energy is calculated by considering both bending and membrane deformation during the folding process. FE simulations are used to evaluate the force-displacement response, specific energy absorption, crush pattern, and crush distance for different multi-cell, multi-corner models. The geometric features of interest include the arrangement of the interior walls and their connectivity with the outer tube walls that result in acute or obtuse angles. The analytical predictions for the mean crush force are found to be in good agreement with the FE solutions. Results also show a strong correlation between the cross-sectional geometry and the crash behavior with the method of connecting the inner to the outer walls having large influence on the energy absorption.

I. Introduction

SAFETY is one of the most important criteria in design of automotive structures. In general, a crashworthy vehicle must meet the impact energy management criteria that require the passenger compartment structure to sustain crash loads without excessive deformation while absorbing and dissipating the kinetic energy of impact. Some automotive structural components such as the side rails play a vital role in absorbing the bulk of impact energy in full- and offset-frontal crash conditions.[1] With the goal of minimizing injury to the vehicle occupants as defined by the head injury criteria (HIC)[2], the design of side rails requires a proper balance between intrusion distance and peak acceleration. While the component has to be stiff enough to limit intrusion, it has to accommodate sufficient plastic deformation to attenuate the impulsive force and associated acceleration transferred to the occupants. Besides the engineering properties of the material, the geometric attributes of the side rail can have a significant impact on its collapse characteristics. By controlling the form and rate of plastic deformation during impact, it would be possible to increase energy absorption and reduce peak acceleration. Crush zone, the portion of the side rail allowed to deform under crash loads, can extend from a fraction to the entire length of the component. In its generic form, a side rail can be represented as a thin-walled prismatic column whose geometric attributes are limited to its cross-sectional shape and dimensions.

Over the past thirty years, numerous experimental, analytical, and numerical studies have been conducted to gain better understating of the crushing mechanism of thin-walled tubular components and evaluation of their characteristics in terms of the mean crush force, folding deformation, and energy dissipation associated with progressive plastic collapse under static and dynamic axial compression. These studies have principally focused on prismatic columns made of steel and aluminum with some having foam-filled cavities.[3,4]

Analytical methods originated from the pioneering works of Alexander[5] on cylindrical tubes and those of Wierzbicki and Abramovicz[6-8] on multi-corner tubes. Experimental studies by Abramowicz and Jones[9] on square tubes made of mild steel showed the existence of various crush mode shapes including two symmetric and two asymmetric modes. Motivated by the kinematics of crushing observed in experimental studies, the analytical methods consider the mechanics of progressive collapse associated with the bending and membrane deformation in

[1] Graduate Research Assistant, Student Member, AIAA.
[2] Professor, Associate Fellow, AIAA.

the component. Through careful examination of the collapsing response, Wierzbicki and Abramowicz[6-8] proposed a super folding element (SFE) model whereby a corner portion of the cross-section is represented in terms of eighteen separate members whose characteristics are described in terms of the three principal folding mechanisms: *inextensional*, *quasi-inextensional*, and *extensional* deformations. The key aspect of SFE is the recognition of the formation and propagation of various hinge lines that define the boundaries of the constituent members. SFE was used to predict the mean crush force of multi-corner tubes and to show that there is no considerable difference between the crush force in asymmetric and symmetric collapse modes.[9] Jones[10] also concluded that because of the small difference between the two different classes of mode shapes, either mode could occur in physical experiments. It is worth mentioning that wall thickness can also affect the crush mode.[11,12] Because of the difference in deformation patterns, tubular columns with medium side-to-thickness ratio show a *compact* crush mode whereas for the thin-walled tubes, the mode is *non-compact*.

Although both static and dynamic tests have been used to measure the crushing response, the effect of dynamic load on the material properties is often ignored in analytical solutions. In 1989, Weirzbicki and Abramovicz[7] modified the SFE model to capture the strain rate effect in strain rate sensitive materials. They used the relationship that was previously proposed by Cowper and Symonds[13] based on testing of different metallic materials at various strain rates. This phenomenological relationship, which modifies the yield stress for different strain rates, has also been incorporated into many nonlinear finite element codes such as LS-DYNA for including the effect of strain rate on classical plasticity models. Langseth and Hopperstad[14] performed extensive experiments on different heat-treated square aluminum tubes under both static and dynamic loadings, and showed that in static testing, most of the mode shapes are symmetric whereas in dynamic cases, the mode shape tends to vary during the crushing deformation. They also observed that the mean crush force for dynamic cases are higher than the static ones, and concluded that by introducing imperfection, the ratio between dynamic and static mean crush force can be kept constant. Hansen et al.[15,16] experimentally showed that the dynamic effect causing an increase in the mean crush force of strain-rate-insensitive aluminum is because of inertial force arising from the acceleration of extrusion walls introduced by dynamic loading. In 1998, Jones[10] classified the crushing behavior into *static plastic buckling* (which considers the post-buckling of thin-walled columns under static or quasi-static loads), *dynamic progressive buckling* (where all the crushing progression is confined to one end of a dynamically crushed column), and *dynamic plastic buckling* (where shell is wrinkled over the entire length). The last two classes of crushing are distinguished by the initial impact velocity and the mass ratio between the impactor and the column. Although the distinction between these two classes also depends on the material and geometric properties of the column, the dynamic plastic buckling[17] occurs for impact velocities higher than 100 m/s and mass ratio of 600. In most of the studies related to automotive crashworthiness, the behavior is in the range of dynamic progressive buckling.

By the late 1980s and the development of nonlinear finite element analysis (FEA) codes such as LS-DYNA and PAM-CRASH, it became possible to analyze the crash phenomenon[18,19] as a non-smooth, highly nonlinear problem based on the explicit time integration technique. Most of the element models used in these codes where originally developed by Belytschko et al.[20] and Hughes et al.[21,22] with subsequent modifications aimed at correcting the problem of zero energy (hourglass modes), enhancing the computational efficiency and rate objectivity, and patch tests. In the case of contact-impact analysis for dynamic progressive buckling simulations, the penalty method[23] is often used for rigid body and self contact calculations. To include material nonlinearity, many previous studies have used classical elastic-plastic models with kinematic and/or isotropic hardenings.[24] As mentioned earlier, these methods can also include the Cowper-Symonds[25] model to account for strain rate sensitive materials.[26]

One way to control the crush zone and plastic deformation of columns is through the design of multi-cell cross-sections. Component production using the extrusion process makes it possible to easily manufacture various prismatic components multi-cell, multi-corner cross-sectional configurations. Previous studies by Santosa[27,28], Chen and Wierzbicki[3], Kim[29], and Zhang, et al.[30,31] showed that multi-cell rectangular profiles with more corners can enhance the energy absorption capacity of columns. Chen and Wierzbicki[3] modified the mean crush force formulation of simple multi-cell rectangular tubes to account for the addition of foam material used to fill the open spaces inside the column. Their method resulted in an analytical equation for the mean crush force based on the division of the cross-section into a number of flange elements, the cross sectional area, and the plastic flow stress. Their results indicated that the foam-filled tubes generally had (~30%) higher specific energy absorption (SEA) than the corresponding empty-cell tubes while the addition of interior walls (double and triple cell models) increased the SEA value by about 15% in comparison to the single cell model. Zhang et al.[30,31] introduced a simple way for mean crushing force calculations based on SFE concept deformation results obtained from FE simulations. They divided the multi-cell rectangular cross section into a number of 2-flange corners, 4-flange cruciform, and 3-flange T-shaped elements, and estimated the combined contributions of these elements to the internal energy and the mean crush force. Zhang and Suzuki[32] studied the effect of different types of longitudinal and transverse stiffening of square

tubes. They also developed an equation for mean crush force by accounting for stiffener effects and modifying the thickness parameters appearing in previous studies.

In all of the previously cites investigations, the cross-sectional shapes considered were limited to either single cell (circular, rectangular, hexagonal, or rhomboidal) or multi-cell tubes with identical (rectangular or hexagonal) cell properties. In this paper, we extend the SFE model of Wierzbicki[8] to investigate the crush characteristics of multi-cell tubes consisting of two different types of three-flange elements characterized by either two obtuse or two acute angles separating the three flanges. A closed form equation for prediction of mean crush force is developed. Moreover, a series of FEA simulations are conducted to analyze the influence of cross-sectional geometry on the collapsing mechanism, local and global progressive folding response, energy absorption, and crush force for a number of example problems. Four different metrics are used to compare the efficiency and performance of the selected models. The values of mean crush force based on different analytical equations as well as FEA simulations are compared and analyzed.

The remaining portion of the paper is organized as follows. The mechanics of progressive plastic collapse and the modification of SFE model are discussed in Section 2. Finite element modeling and simulation description is given in Section 3. Results of the example problems are discussed in Section 4 followed by some concluding remarks.

II. Mechanics of Progressive Plastic Collapse

Crushing deformation of thin-walled multi-corner columns under quasi-static and dynamic axial loads is principally governed by the collapse mechanism of the corner sections. Following a careful examination of the folding mechanisms present in a deforming corner section of various tubes made of ductile materials, Wierzbicki and Abramovicz[6] developed a super folding element (SFE) model based on the theory of plasticity. They concluded that the collapse phenomenon is a progressive failure that can be represented in terms of angle α and described by quasi-inextensional and extensional folding modes as depicted in Fig. 1(a) and (b). Each fold is defined in terms of the half-length *H*, the corner angle $2\pi - \psi_0$, and wall thickness *t*. In their generalized folding model shown in Fig. 1(c), they identify the formation of 18 shell elements that are combined into five separate groups depending on their response characteristics. These elements are identified as: groups 1 and 2 consist of cylindrical and conical surfaces that have floating boundaries and undergo inextensional deformation; element 3 is a toroidal surface with moving boundaries and quasi-inextensional deformation; group 4 consists of conic surfaces that undergo extensional deformation; and group 5 represents multiple trapezoidal elements that undergo rigid-body translation and rotation due to propagating hinge lines. What is clear in this model is that despite the drastic geometric distortion, the crushing process is characterized by localization of plastic deformation in a relatively small area of the structure.

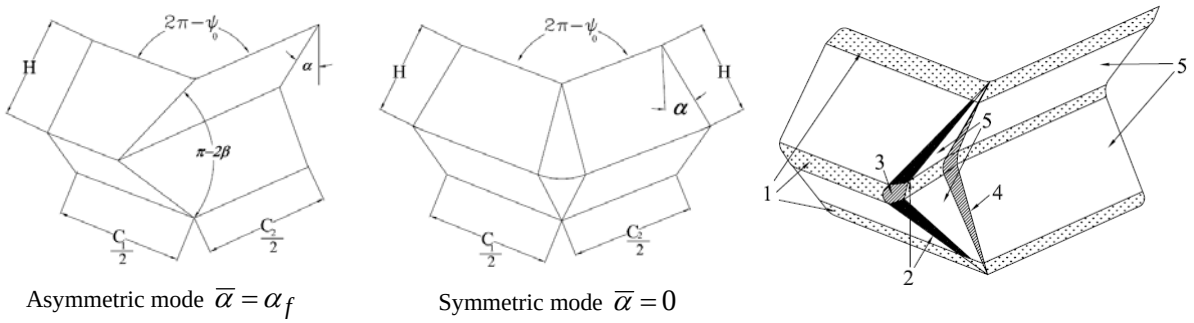

Asymmetric mode $\bar{\alpha} = \alpha_f$ Symmetric mode $\bar{\alpha} = 0$

Figure 1. (a) Quasi-inextensional mode, (b) extensional mode, and (c) super folding element model.

The angle parameter $\bar{\alpha}$ ($0 \le \bar{\alpha} \le \alpha_f$) defines the contribution of extensional mode to the total energy dissipation. When $\bar{\alpha}$=0, the folding mode is completely symmetric whereas for $\bar{\alpha} = \alpha_f$, the folding is purely asymmetric. In SFE, the folding process starts as an asymmetric mode that continues up to a point where the inclined hinge line is locked and the symmetric deformation begins. The actual value of $\bar{\alpha}$ depends on geometric parameters, wall thickness, and the corner angle. The geometry of all of the contributing elements can be fully described by three parameters $\{H, b, \bar{\alpha}\}$, where b is the radius of toroidal surface. These parameters are calculated from the energy balance considering the contribution of each cross-sectional element.

For shells made of rigid-perfectly plastic isotropic materials, the rate of internal energy dissipation is divided into continuous and discontinuous velocity fields[7]

$$\dot{E}_{\text{int}} = \int_S \left(M_{\alpha\beta}\dot{\kappa}_{\alpha\beta} + N_{\alpha\beta}\dot{\varepsilon}_{\alpha\beta} \right) dS + \sum_{i=1}^{m} \int_{L^i} M_o^i \dot{\theta}^i \, d\ell^i \tag{1}$$

where S defines the extent of continuous plastic deformation, L^i is the length of the ith hinge line, m is the total number of stationary or moving hinge lines. In the continuously deforming zones, bending moments $M_{\alpha\beta}$ and membrane forces $N_{\alpha\beta}$ are the conjugate generalized stresses for the components of the rotation rate tensor $\dot{\kappa}_{\alpha\beta}$ and extension rate tensor $\dot{\varepsilon}_{\alpha\beta}$. $M_o^i = \sigma_o t^2/4$ is the fully plastic bending moment per unit length with σ_o representing the flow stress found as $\sigma_o = \sqrt{\sigma_y \sigma_u/(1+n)}$, where σ_y and σ_u represent the yield strength and ultimate stress of the material, respectively, with *n* as the exponent of the power law.

The total internal plastic energy is obtained by integrating Eq. (1) in the interval range of $0 \le \bar{\alpha} \le \alpha_f$. Since deformation is based on two different folding modes that are assumed to develop in series[6-8], the expression for the internal energy is divided into two parts and calculated as

$$E_{\text{int}} = \int_0^{\bar{\alpha}} \dot{E}_{\text{int}}^{(1)} d\alpha + \int_{\bar{\alpha}}^{\alpha_f} \dot{E}_{\text{int}}^{(2)} d\alpha \tag{2}$$

The two integrals in Eq. (2) can be decomposed as $\int_0^{\bar{\alpha}} \dot{E}_{\text{int}}^{(1)} d\alpha = E_1 + E_2 + E_3$ and $\int_{\bar{\alpha}}^{\alpha_f} \dot{E}_{\text{int}}^{(2)} d\alpha = E_4 + E_5 + E_6$ where E_i defines the contribution of each folding mechanism to the energy dissipation and is calculated here by considering the separate portions of the cross section as

$$E_1(\psi_0, \bar{\alpha}) = 16 M_{01} I_1(\psi_0, \bar{\alpha}) \frac{Hb}{t_{av}} \qquad \text{(toroidal surface)} \tag{3}$$

$$E_2(\bar{\alpha}, C_1, C_{sh}) = 2 M_{02} C_1 \bar{\alpha} + 2 M_{03} C_{sh} \bar{\alpha} \qquad \text{(horizontal hinge lines)} \tag{4}$$

$$E_5(\bar{\alpha}, \alpha_f, C_1, C_{sh}) = 2 M_{02} C_1 (\alpha_f - \bar{\alpha}) + 2 M_{03} C_{sh} (\alpha_f - \bar{\alpha}) \qquad \text{(horizontal hinge lines)} \tag{5}$$

$$E_3(\psi_0) = 4 M_{01} I_3(\psi_0) \frac{H^2}{b} \qquad \text{(inclined hinge lines)} \tag{6}$$

$$E_4(\psi_0) = 4 M_{03} I_4(\psi_0, \bar{\alpha}) \frac{H^2}{t/2} \qquad \text{(conical surfaces)} \tag{7}$$

$$E_6(\psi_0, \bar{\alpha}) = M_{01} H I_6(\psi_0, \bar{\alpha}) \qquad \text{(inclined hinge lines)} \tag{8}$$

with

$$I_1(\psi_0, \bar{\alpha}) = \frac{\pi}{(\pi - 2\psi_0)\tan\psi_0} \int_0^{\bar{\alpha}} \cos\alpha \left\{ \sin\psi_0 \sin\left(\frac{\pi - 2\psi_0}{\pi} \beta \right) + \cos\psi_0 \left[1 - \cos\left(\frac{\pi - 2\psi_0}{\pi} \beta \right) \right] \right\} d\alpha \tag{9}$$

$$I_3(\psi_0) = \frac{1}{\tan\psi_0} \int_0^{\bar{\alpha}} \frac{\cos\alpha}{\sin\gamma} d\alpha \tag{10}$$

$$I_4(\psi_0,\overline{\alpha}) = \int_{\overline{\alpha}}^{\alpha_f} \left\{ \frac{\sin\overline{\alpha}\sin 2\alpha \tan\psi_0}{2(\sin^2\overline{\alpha} + \tan^2\psi_0 \sin^2\alpha)} + \left(\frac{\pi - 2\psi_0}{\pi}\beta\right)\cos\alpha \right\} d\alpha \tag{11}$$

$$I_6(\psi_0,\overline{\alpha}) = \frac{2}{\tan\psi_0} \int_{\overline{\alpha}}^{\alpha_f} \frac{\sin\overline{\alpha}(\sin^2\overline{\alpha} + \tan^2\psi_0)}{\sin^2\overline{\alpha} + \tan^2\psi_0 \sin^2\alpha} d\alpha \tag{12}$$

where the angles $\alpha, \beta,$ and ψ_0 are defined in Fig. 1 while flange dimensions C_1 and C_{sh} are defined in Fig. 2.

To preserve energy balance, the total internal energy defined by the sum of individual contributions from Eqs. (3)-(8) has to be equal to the external work done by the axial crushing force and defined as

$$E_{ext} = \int_0^{t_f} \dot{E}_{ext} dt = P_m \int_0^{t_f} \dot{u}_0 dt = P_m \delta_e \tag{13}$$

where P_m is the mean crush force and δ_e the associated effective axial deformation, which is set later to be equal to 0.73(2*H*) as observed in crush tube experiments.[9,14] The mean crush force depends on three primary parameters $\{H, b, \overline{\alpha}\}$ and is found using the minimum conditions[33]

$$\frac{\partial P_m}{\partial H} = 0 \ , \ \frac{\partial P_m}{\partial b} = 0 \text{, and } \frac{\partial P_m}{\partial \overline{\alpha}} = 0 \tag{14}$$

A. Multi-cell prismatic columns

Figure 2 Illustrates four different multi-cell configurations. When divided into its distinct corner sections, each cross-section is characterized by two- and three-flange elements. The two-flange elements are described by the width dimensions C_1 and C_2 whereas the three-flange elements include an additional flange with width C_{sh}. All members have the same thickness, *t*. Table 1 shows the distribution of decomposed elements in multi-cell models A, B, C, and D.

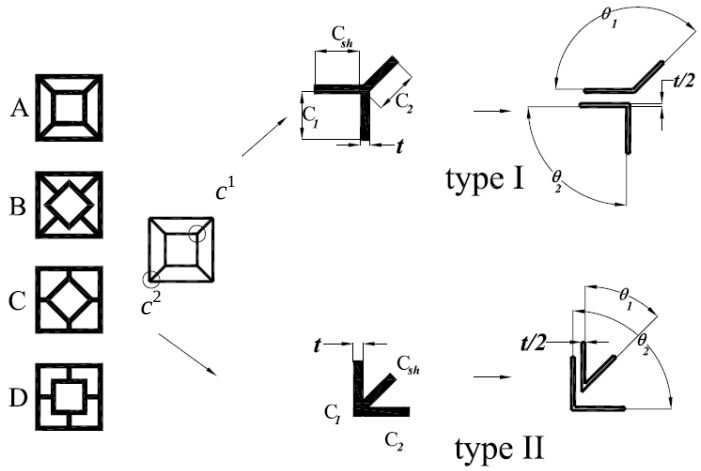

Figure 2. Alternative cross-sectional models for multi-cell columns.

Two types of three-flange elements, identified as types I and II in Fig. 2, are considered. Type I element has two obtuse angles while type II has two acute angles. Simple T elements present in models C and D are treated as type I. For analysis purposes, the three-flange elements are split into separate two-flange elements with the dividing line along the centerline of the shared flange, C_{sh}. This decomposition produces a different thickness for the shared flange and changes the plastic bending moments in Eqs. (3)-(8) to $M_{01} = \frac{\sigma_0 t_{av}^2}{4} = \frac{\sigma_0 (3t/4)^2}{4} = \frac{9\sigma_0 t^2}{64}$; $M_{02} = \frac{\sigma_0 t^2}{4}$; and $M_{03} = \frac{\sigma_0 t^2}{16}$. Taking $\alpha_f = \pi/2$, a generalized two-flange element model emerges with the total internal energy obtained as

$$E_{\text{int}}{}^{2\psi_0} = E_1(\psi_0,\overline{\alpha}) + E_2(\overline{\alpha}, C_1, C^*) + E_3(\psi_0) + E_4(\psi_0) + E_5(\overline{\alpha}, \frac{\pi}{2}, C_1, C^*) + E_6(\psi_0,\overline{\alpha}) \tag{15}$$

where $C^* = C_{sh}$ for each portion of a three-flange element and $C^* = C_2$ for a stand-alone two-flange member. For a two-flange element with flanges separated by a 90º angle, Eq. (15) gives $E_{\text{int}}{}^{2\psi_0} = E_{\text{int}}{}^{(\pi/2)}$. For a three-flange element, Eq. (15) is used according to the decomposition shown in Fig. 2 resulting

Table 1: Distribution of corner elements in multi-cell tubes.

Model	No. of 2-flange elements	No. of 3-flange elements (type I)	No. of 3-flange elements (type II)
A	0	4	4
B	4	4	4
C	4	8	0
D	8	8	0

in $E_{\text{int}}{}^{2\psi_0} + E_{\text{int}}{}^{2\psi_0'}$. For a type I corner such as c^1 in Fig. 2, $E_{\text{int}}^{c^1} = E_{\text{int}}^{(\pi/2)} + E_{\text{int}}^{(3\pi/4)}$ while for corner c^2 (type II), $E_{\text{int}}^{c^2} = E_{\text{int}}^{(\pi/2)} + E_{\text{int}}^{(\pi/4)}$. It is important to note that each angle θ in Fig. 2 is related to angle ψ_0 such that $2\psi_0 = \pi - \theta$. The total energy dissipation for multi-cell models A through D can be obtained by adding the contribution of individual corner elements, which together with Eq. (14) provides a closed form formula for the mean crush force as

$$P_m = \frac{1}{1.46H} \sum_{j=1}^{n_e} N_j E_{\text{int}}^j \tag{16}$$

where N_j represents the number of each distinct corner elements with separate contributions to the total energy absorption of the column, and n_e represents the number of element types present in the cross-section. Since Eq. (16) is based on a single value for half-distance, H, some error will be introduced in the estimated value of P_m for crush cases with non-uniform fold geometries.

Equation (16) is derived for the quasi-static crushing condition. To account for the inertia and strain-rate effects in dynamic crushing, the calculated mean crush force from Eq. (16) has to be multiplied by an appropriate amplification coefficient as proposed by Langseth and Hopperstad.[14] Based on various crushing experiments with square tubes made of AL6060-T4 aluminum, the amplification coefficient is shown to be in the range of 1.2 to 2.0.[14-16] It is worth noting that for aluminum tubes, the amplification factor is dominated by the inertia effects.

B. Metrics of crush characteristics

The performance characteristics of various multi-cell designs are compared using four different metrics. Hanssen et al.[16] The ratio of global deformation to the length of the column defines the deformation capacity metric defined as $D_c = \delta / l$. The specific energy absorption is the ratio of total energy absorption to total mass defined as $SEA = E_{\text{int}}^T / \rho A l$. The ratio of average crush force and maximum crush force in a specified interval of deformation is defined as the crush force efficiency defined as $A_E = E_{\text{int}}^T(\delta) / [P_{\max}(\delta)\delta]$. The total efficiency can be used as a measure of energy absorption capacity and is defined as $T_E = A_E D_c$. Eventually, the relative deformation D_c at which T_E reaches its maximum value is referred to as the effective crushing distance, δ_e of the column.

III. Numerical Simulations of Collapse Response

Two different dynamic loading simulation cases have been considered. In case1, a tube with a distributed aft-end mass of 300 kg and traveling at a speed of 15.6 m/s (35 mph) strikes a rigid wall whose contact surface is perpendicular to the axis of the tube (direction of motion). In case 2, tube is held fixed at its base and is struck at the other end by a 300-kg rigid block (hammer) traveling at a speed of 15.6 m/s as shown in Fig. 3. In case 1, the contact friction coefficient between the rigid wall and tube is set at 0.3. To prevent element-element penetration due to excessive deformation, a frictionless self-contact condition has been specified for the element surfaces. All tube models analyzed here are made of AL6060-T6 (E = 70 GPa, ν = 0.3, and ρ = 2.7e-6 kg/mm^3) with true stress-strain curve shown in Fig. 4.

Element density study has been performed to obtain an optimum mesh density for the models investigated. Because of the high distortion in elements, zero energy deformation or hourglass energy is calculated for element performance check. Results show a very small non-physical hourglass energy that is less than 2% of the total internal energy.

The FE models used here are developed using the ANSYS-preprocessor with FEA simulations performed using transient dynamic nonlinear explicit FE code LS-DYNA. All simulations are conducted on 16 nodes of

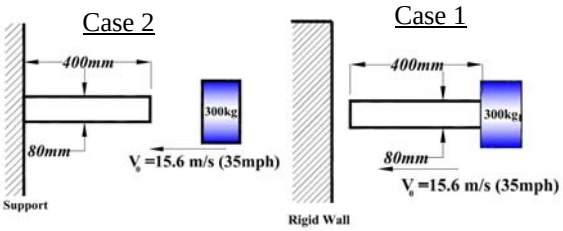

Figure 3. Description of the two dynamic loading cases considered.

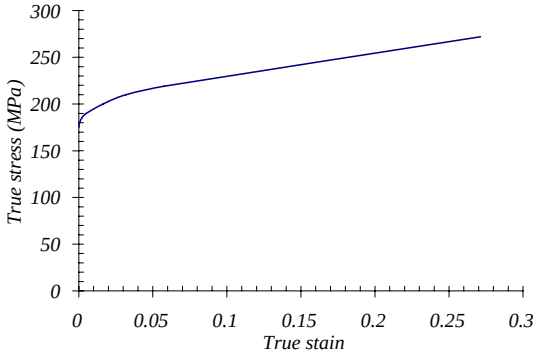

Figure 4. True stress-strain curve of the selected material.

RAPTOR, a 2048 processor cluster composed of 512 Sun Microsystems SunFire X2200 M2 servers, each with two dual-core AMD Opteron 2218 processors (2.6GHz) and 8 GB of memory (for a total of 4TB) at Mississippi State University. The post-processor LSPREPOST is used for visualization and data acquisition. To filter out noise in the simulation results, the SAE type filtering with the frequency of 60 Hz has been used.[25] The termination time has been specified at 50 ms for all the cases considered.

A. Effect of element type

Prior to establishing a baseline model for crush characteristics of multi-cell columns, the effect of element type on collapse response of a simple square tube model was investigated using the explicit nonlinear FEA code, LS-DYNA. A list of available shell elements in LS-DYNA and their major properties are given in the appendix.

The square tube cross-sectional dimension is 80 mm with wall thickness of 2 mm and length of 400 mm. The model is analyzed using the case 1 loading condition and without introducing any imperfection. The results are shown Fig. 5 with the top end representing the impact side of the tube. Figure 5 shows that the predicted collapse mode shapes are different. However, the calculated crush force dissipation is nearly the same for all the selected element types.

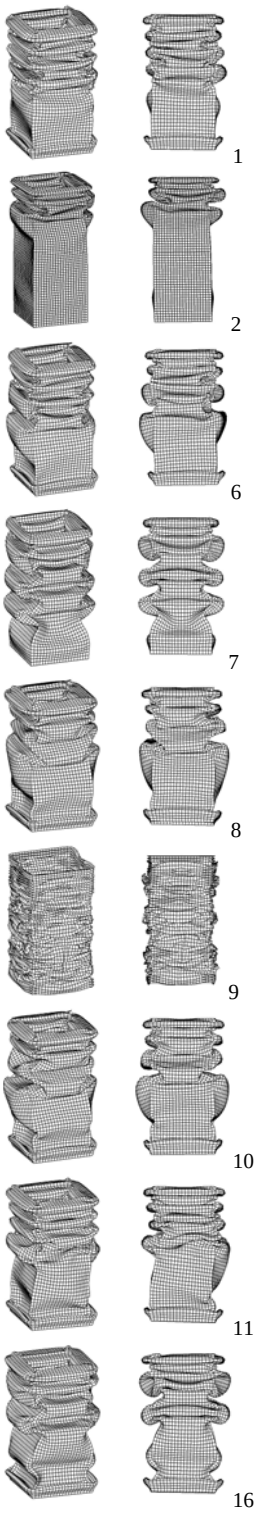

Figure 5. Crush response for different element types.

B. Effect of trigger mechanism

Trigger mechanism is used to lower the initial peak crush force, induce a stable progressive failure, and produce a symmetric crush mode in columns. In this study, a simple trigger mechanism in the form of small indentation on two opposite walls is used. The location of the indentation trigger relative to the impacted end of the tube is varied from 5 mm to 30 mm with the effect on the crush force dissipation shown in Fig. 6.

It is clear that the addition of indentation trigger reduces the initial peak force while stabilizing the deformation as indicated by the shapes of the curves. However, the location of the trigger in the range tested is found to be less important, with the trigger location of 15 mm giving a slightly higher mean crush force than those at 5 and 30 mm.

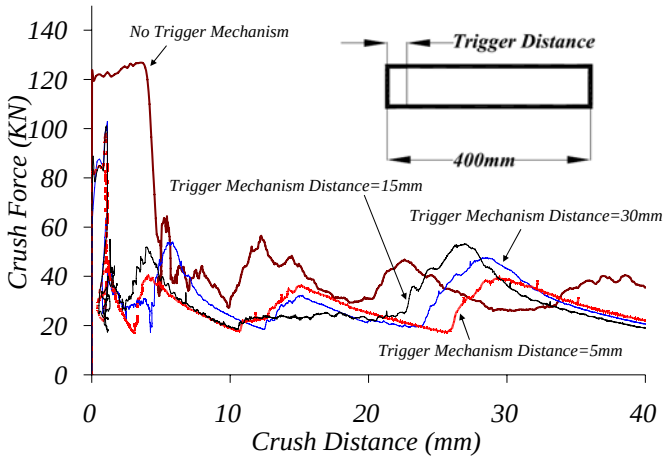

Figure 6. Crush force variation as a function of trigger location.

IV. Results and Discussion

The results of this investigation focus mainly on evaluation of multi-cell columns possessing type I and II corner geometries with models A through D in Fig. 2 as four possible examples. The selected models generally show a square inner tube connected to a square outer tube twice its size. The distinguishing feature is the way the inner and outer tubes are connected together to form the multi-cell geometry. The connecting webs create *corner-to-corner*, *web-to-corner*, *corner-to-web*, and *web-to-web* attachments in these models. Although the shape and dimensions of the inner and outer tubes are identical in all four models, there is a slight weight difference due to minor variation in width dimensions of

connecting webs. Since energy absorption and the stability of progressive folding are heavily dependent on the corner elements,[29] the four configurations can produce different crushing characteristics. The wall thickness is kept constant at 2mm with the outer and inner tubes having a side dimension of 80 mm and 40 mm, respectively. The length of the tube is 400 mm. Based on the power law relation and the material properties[34] (σ_y = 175 MPa, σ_u = 206 MPa, and n = 0.1), the resulting flow stress is found to be σ_o = 181 MPa.

All FE models are based on Hughes-Liu shell elements[26] using the case 2 dynamic loading condition and associated parameters discussed in the previous section. An indentation trigger mechanism has been introduced on two opposite walls of the outer tube. The progressive collapse mode shapes of tube models A through D are shown in Fig. 7 at various time increments up to 30 ms. The instantaneous values of crush force and crush distance at t = 30 ms are also shown for comparison.

All models undergo stable progressive collapse with repeated folding deformation that extends to nearly 75% of the length in model D and the entire length in model A. Clearly, model A demonstrates less resistance to axial deformation as compared to model D, indicating the difference between corner-to-corner and web-to-web connections. Also, models B and C appear to have nearly the same deformation length while the folding geometries of the two models are distinctly different.

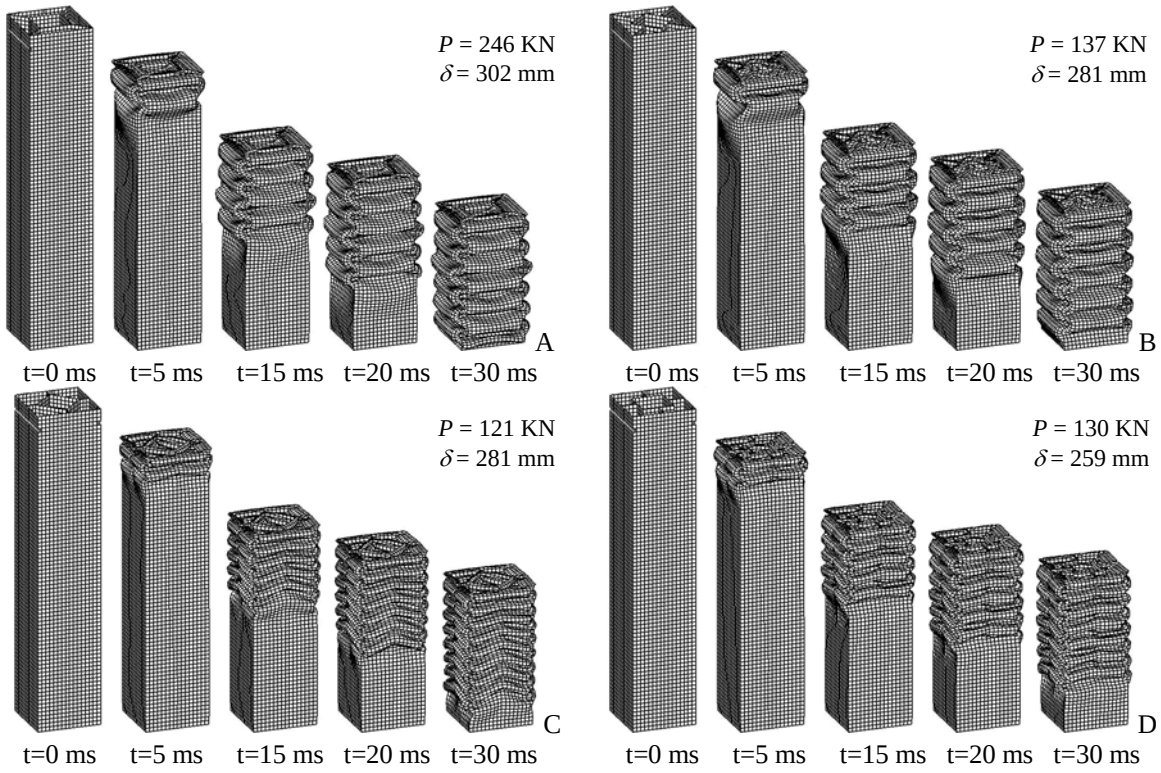

Figure 7. Progressive collapse of multi-cell tube models A, B, C, and D (deformation scale factor = 0.8).

In Fig. 8, close up views of the inner tubes in these four selected models are shown. For models B and D with web-to-corner and web-to-web connections, the crush mode is more complicated. In model A, the mode shape is asymmetric while in model C, the mode shape is symmetric with two opposite corners deforming in a same fashion, one inward and the other outward. In model D, the overall behavior is

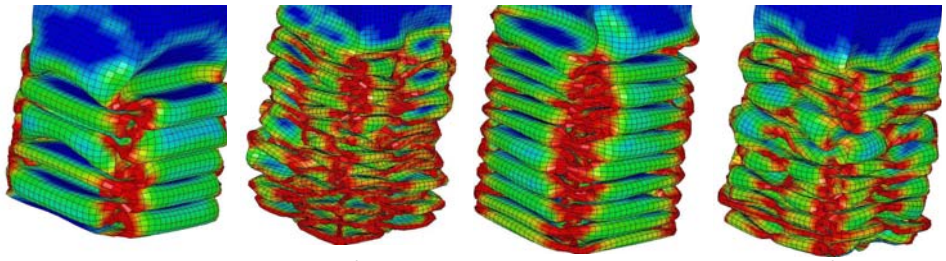

Figure 8. Deformed shapes of the inner tubes in models A, B, C, and D.

close to asymmetric type of deformation, but it is not uniform and the crush distance varies during the crush process. A more complicated mode shape is seen in model B where there is a combination of various mode shapes. At the beginning, it behaves close to symmetric mode and then it changes into a non-uniform shape that results in folding and heavy distortion of the T shape sections. Keeping the non-uniform crush distance the folding change their mode to a shape that is close to asymmetric mode shapes. As seen here, the crush modes in some of the models are not similar to the classical deformation patterns observed in simple rectangular tubes. These complex mode shapes are not considered in the analytical method discussed in Section2, which is based on predictive kinematics of crushing phenomenon associated with distinct quasi-inextensional and extensional folding mechanisms.

The plots of crush force versus crush distance are shown in Fig. 9. Besides the multi-cell models A through D, other models are also analyzed with results shown for comparison. Model F represents a square tube. Models G and H are the same as those previously analyzed by Chen and Wierzbicki[3] whereas models E and I are those examined by Zhang et al.[30,31] The initial peak force in models C and D are slightly less than those in A and B. This shows that models A and B are less rigid than C and D. The progressive collapse characteristics in the four selected models are clearly evident in this plot.

The plots of average crushing force for all nine models are shown in Fig. 10. Given the range of values for the average crush force, it is possible to label models F, G, and H as "soft", models I, A, B, C, and D as average or "mild", and model E as "hard". Based on the geometric attributes and crush characteristics of those models in the mild category, they appear to be good candidates for design optimization.

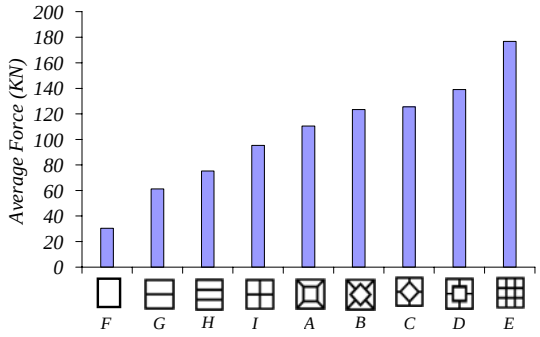

Figure 10. Average crush force for various models.

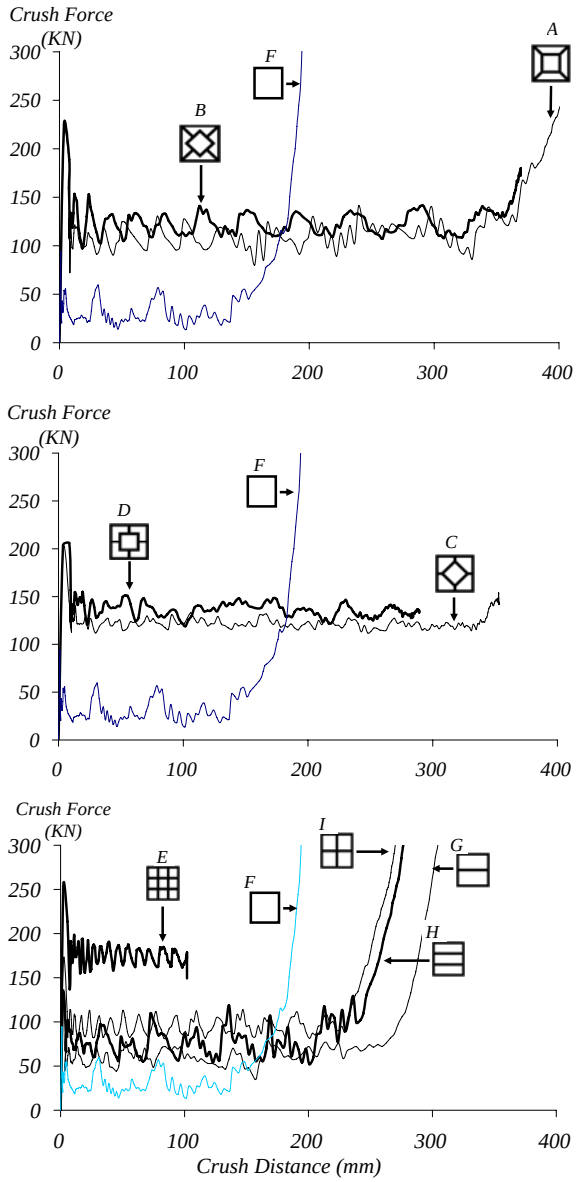

Figure 9. Crushing force variations for single-cell and multi-cell tubes with different cross-sectional geometries.

The simulation-based results for average crush force are compared with the analytical predictions in Table 2. The analytical models in Chen and Wierzbicki[3] and Zhang et al.[30] were applied to single-cell and multi-cell tubes with the intersecting walls having an orthogonal arrangement.

For the application of Chen and Wierzbicki's equation, models A through D are divided into m separate flanges with the material cross-sectional area denoted as A resulting in the average crush force formula: $P_m = 1.22(2/3)\sigma_0 t\sqrt{\pi m A}$. For the Zhang et al.'s equation, type I and II corners are treated as simple T-shape elements. With the number of two-flange elements denoted as N_1 and three-flanges as N_2 (for type I) and N_3 (for type II), the formula for the average crush force

becomes $P_m = 1.22\sigma_0 t\sqrt{(N_1 + 2N_2 + 2N_3)\pi t L_c}$. For the two analytical equations above as well as that in Eq. (16), a dynamic amplification coefficient of 1.22 is used. This coefficient is near the low end of the range of 1.2 to 2.0 suggested by Langseth and Hopperstad[14] due to the presence of trigger mechanism in the tube models.

For models B and D with web-to-corner and web-to-web inter-wall connections, the mean crush force predictions by Eq. (16) are found to be fairly accurate. However, for models A and C with corner-to-corner and corner-to-web inter-wall connections, analytical results are less accurate than the simulation-based results.

Table 2: Comparison of numerical and analytical predictions for various multi-cell tubes.

	Average Force, KN (%error)			
Model	Simulation	Chen-Wierzbicki[3]	Zhang et al.[30]	Present study
A	110	88 (20)	76 (31)	92 (16)
B	125	105 (15)	124 (1)	126 (2)
C	123	96 (23)	114 (9)	106 (14)
D	139	111 (20)	128 (8)	139 (~0)

Total efficiency and specific energy absorption plots are shown in Fig. 11. The results for the other multi-cell configurations are also presented for comparison. In terms of total efficiency, it can be seen that models F through I cannot properly absorb the kinetic energy. Because of high stiffness, model E also is not efficient while the models A through D can absorb energy through progressive collapse reaching nearly the entire length. This will be critical when we have design constraint on length of the tube. In terms of specific energy absorption, models A through D show greater capacity than the baseline and the other configurations.

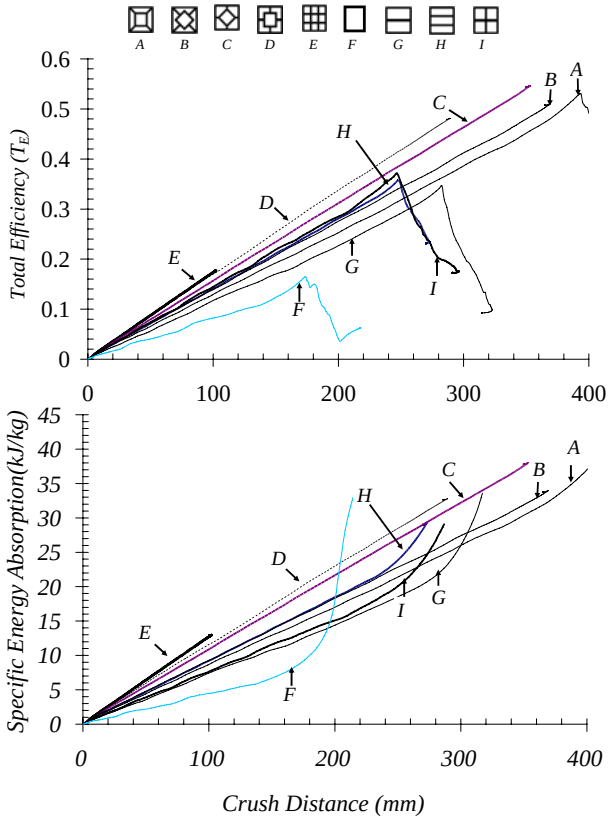

Figure 11. The values of selected metrics for energy absorption.

V. Conclusions

An analytical formula for the prediction of mean crush force was derived based on the super folding element model and the associated kinematically consistent representation of plastic collapse in the corner regions. This formula together with nonlinear transient dynamic finite element (FE) simulations were used to study the influence of cross-sectional geometry on the crush characteristics of multi-cell prismatic columns made of ductile materials. Force-displacement response, specific energy absorption, crush pattern, and crush distance for different multi-cell, multi-corner models were investigated. The geometric features of interest included the arrangement of the interior walls and their connectivity with the outer tube walls that resulted in acute or obtuse angles.

The study of the kinematics of crush in the multi-cell tubes shows that the method of connecting the inner and outer walls plays a crucial role in determining the crush mode (ranging from asymmetric or symmetric to mixed and non-uniform deformation), the crush distance, and the accuracy of the analytically predicted mean crush force. The analytical predictions of the mean crush force for models with web-to-corner and web-to-web inter-wall connections are much better than those for the other two models. The irregularity of the folding patterns is one reason for this discrepancy. Both FE and analytical results show that the new multi-cell models have approximately 3 to 5 times greater mean crush force than that of the single-cell square tube with nearly twice the specific energy absorption. Also from the analysis of total energy absorption efficiency, it can be concluded that the new multi-cell models have a greater capacity to absorb impact energy than the other multi-cell models with rectangular cell geometry.

Appendix

List of shell elements investigated in this study.

LS-DYNA Element Number	Name	Properties
1	*Hughes-Liu*	Degeneration of 8node brick, incrementally objective, uniformly reduced integration, nonplanar geometry, one point quadrature
2	*Belytschko-Tsay (Lin)*	Computationally efficient, 5 through-the-thickness integration points, co-rotational coordinates and rate of deformation formulation, hourglass viscosity, nonplanar geometry, Hughes-Liu mass matrix
6	*S/R Hughes-Liu*	Selectively reduced integration near boundary and point loads to prevent hourglass, nonplanar geometry
7	*S/R co-rotational Hughes-Liu*	Similar to element 6 using co-rotational coordinate system from Belytschko-Tsay
8	*Belytschko-Leviathan*	Modified Belytschko-Tsay for passing the patch test, physical hourglass control
9	*LS-DYNA*	Fully integrated Belytschko-Tsay (element type 2)
10	*Belytschko-Wong-Chiang*	Perfectly planar geometry
11	*LS-DYNA*	Fast co-rotational Hughes-Liu (element type1)
16	*LS-DYNA*	Fully integrated Shell

Acknowledgements

The funding provided for this study by the US Department of Energy under Grant No. DE-FC26-06NT42755 is gratefully acknowledged.

References

[1.] Chung, T.E., Lee, Y.R., Kim, C.S., and Kim, H.S., "Design of Aluminum Space Frame for Crashworthiness Improvement," Document Number: 960167, Feb 1996, SAE international.

[2.] Mahmood, H.F., and Aouadi, F., "Characterization of Frontal Crash Pulse," Crashworthiness, Occupant Protection, and Biomechanics in Transportation Systems-2000, AMD-Vol. 246/BED-Vol49.

[3.] Chen, W. and Wierzbicki, T., "Relative Merits of Single-Cell, Multi-Cell and Foam-Filled Thin-Walled Structures in Energy Absorption, " *Thin-Walled Structures*, Vol. 39, No. 4, 2001, pp. 287-306.

[4.] Kim, H. S., Chen W., and Wierzbicki T., "Weight and Crash Optimization of Foam-Filled Three-Dimensional "S" Frame," *Computational Mechanics*, Vol. 28, 2002, pp. 417-424.

[5.] Alexander, J.M., "An Approximate Analysis of the Collapse of Thin Cylindrical Shells Under Axial Loading," *The Quarterly Journal of Mechanics and Applied Mathematics*, Vol. 13, No.1, 1960, pp. 10-15.

[6.] Wierzbicki, and T. Abramowicz W., "On the Crushing Mechanics of Thin Walled Structures," *Journal of Applied Mechanics*, Vol. 50, 1983, pp.727-734.

[7.] Jones, N., Wierzbicki, T. (ed), Structural Failures, John Wiley, New York, 1989.

[8.] Abramowicz W., and Wierzbicki T., "Axial Crushing of Multicorner Sheet Metal Columns," *Journal of Applied Mechanics*, Vol.56, 1989, pp. 113–120.

[9.] Abramowicz W., and Jones N., "Dynamic Axial Crushing of Square Tubes," *International Journal of Impact Engineering*, 1984, Vol. 2, No. 2, pp. 179-208.

[10.] Jones N., "Structural Impact, " Cambridge University Press, 1997.

[11.] Reid, S.R., Reddy, T.Y., and Gray, M.D., "Static and Dynamic Axial Crushing of Foam-Filled Sheet Metal Tubes," *International Journal of Mechanical Sciences*, Vol. 28, 1986, pp. 295–322.

[12.] Lu, G. and Tongxi, Y., "Energy Absorption of Structures and Materials, " Woodhead Publishing, 2003.
[13.] Cowper, G. R. and Symonds, P. S., "Strain-Hardening and Strain-Rate Effects In the Impact Loading of Cantilever Beams," Brown University, United, 1957.
[14.] Langseth, M. and Hopperstad, O. S., "Static and Dynamic Axial Crushing of Square Thin-Walled Aluminum Extrusions," *International Journal of Impact Engineering*, Volume 18, No. 7-8, October-December 1996, pp. 949-968.
[15.] Hanssen A. G., Langseth M., and Hopperstad, O. S., "Static and Dynamic Crushing of Square Aluminum Extrusions With Aluminum Foam Filler, " *International Journal of Impact Engineering*, Vol.24, No.4, 2000, pp.347-383.
[16.] Hanssen, A. G., Langseth, M., Hopperstad, O. S., "Optimum Design For Energy Absorption of Square Aluminum Columns With Aluminum Foam Filler, " *International Journal of Mechanical Sciences*, Vol. 43, No.1, 2001, pp. 153-176.
[17.] Lindberg H. E., Florence A. L., "Dynamic Pulse Buckling: Theory and Experiment, " M. Nijhoff, 1987.
[18.] Abramowicz, W., "Thin-Walled Structures As Impact Energy Absorbers," *Thin-Walled Structures*, 2003, Volume 41, Issues 2-3, February 2003, pp. 91-107.
[19.] Otubushin, A., "Detailed Validation of A Non-Linear Finite Element Code Using Dynamic Axial Crushing of A Square Tube," *International Journal of Impact Engineering*, Volume 21, No. 5, May 1998, pp. 349-368.
[20.] Belytschko, T., Liu W. K., and Moran, B., "Nonlinear Finite Elements for Continua and Structures," John Wiley & Sons, New York, 2000.
[21.] Hughes, T. J. R., Nonlinear Dynamic Finite Element Analysis of Shells, Nonlinear Finite Element Analysis in Structural Mechanics, *Proceedings of the Europe-U.S. Workshop, Ruhr-Universitat Bochum, Germany, July 28-31*, 1981, pp.151-168.
[22.] Hughes, T. J. R., Finite Element Method - Linear Static and Dynamic Finite Element Analysis, Prentice-Hall, Englewood Cliffs, 2000.
[23.] Belytschko, T. and Neal M. O., "Contact-Impact By The Pinball Algorithm With Penalty Projection and Lagrangian Methods," *International journal of. Numerical. Methods*, Eng. 31 (1991), pp. 547–572.
[24.] Simo, J. C. and Hughes, T. J. R., Computational Inelasticity, Springer-Verlag, New York, 1998.
[25.] LS-DYNA User's Manual version 971, September 2006, Livermore Software Technology Corporation.
[26.] LS-DYNA Theoretical Manual, May 1998. Livermore Software Technology Corporation.
[27.] Santosa, S. P., "Crash Behavior of Box Columns Filled with Aluminum Honeycomb or Foam," Master's Thesis, Mechanical Engineering, MIT, Cambridge, MA, May 1997.
[28.] Santosa, S. P., "Crashworthiness analysis of Ultralight Metal Structures," Ph.D. Dissertation, Mechanical Engineering, MIT, Cambridge, MA, 1999.
[29.] Kim, H. S., "New Extruded Multi-cell Aluminum Profile for Maximum Crash Energy Absorption and Weight Efficiency," *Thin-Walled Structures*, Vol. 40, No. 4, 2002, pp. 311-327.
[30.] Zhang, X., Cheng, G., and Zhang, H., "Theoretical Prediction and Numerical Simulation of Multi-Cell Square Thin-Walled Structures, " *Thin-Walled Structures*, Vol. 44, No. 11, 2006, pp. 1185-1191.
[31.] Zhang, X. and Cheng, G., "A Comparative Study of Energy Absorption Characteristics of Foam-Filled and Multi-Cell Square Columns, " *International Journal of Impact Engineering*, Vol. 34, No. 11, 2007, pp. 1739-1752.
[32.] Zhang, A. N., Suzuki, K., and Lixue, C., "Effect of Stiffeners On Quasi-Static Crushing of Stiffened Square Tube With Nonlinear Finite Element, " *Journal of Ship Mechanics*, Vol. 9, No. 4, 2005, pp. 61-68.
[33.] Abramowicz, W., "Extermal Paths In Progressive Plasticity", *International Journal of Impact Engineering*, Vol. 18, No 7-8, 1996, pp. 753-764.
[34.] De Kanter, J. L. C. G. ,"Energy Absorption of Monolithic and Fiber Reinforced Aluminum Cylinders," PhD dissertation, Delft University of Technology (TUDelft), The Netherlands, 2006.